Check for updates

Energy &
Environmental
Science

rsc.li/ees

Volume 11
Number 4
April 2018
Pages 719-1000

ISSN 1754-5706

REVIEW ARTICLE
Yuekun Lai, Zhiqun Lin et al
Graphene aerogels for efficient energy storage and conversion

ROYAL SOCIETY
OF CHEMISTRY

ROYAL SOCIETY
OF CHEMISTRY

rsc.li/ees

ARTICLE

Rationally Segmented Triboelectric Nanogenerator with Constant Direct-Current Output and Low Crest Factor†

Pengfei Chen,‡[ab] Jie An,‡[ab] Renwei Cheng,‡[ab] Sheng Shu,[ab] Andy Berbille,[ab] Tao Jiang,*[abc] and Zhong Lin Wang*[abcd]

Despite great potential of triboelectric nanogenerators (TENGs) as a promising energy harvesting technology, their practical applications are still hindered by their pulsed outputs with high crest factor. Here, through a simple and easy method involving electrode misalignment (EM) and circuit connection, an exceedingly stable direct current (DC) multi-phase TENG (MP-TENG) with a high average output power at a constant current is developed. The MP-TENG obtained by rectifying and superimposing TENG units with phase difference in parallel can realize an ultra-low crest factor of 1.05 and an average power increase of 40.1%, compared with conventional single-phase TENG. Besides, when using rotor grids with different sizes from the electrodes and EM method, the common materials in daily life such as wood and cloth fabrics have been applied to generate DC-like outputs with a crest factor of less than 1.1, which expands dramatically the selection range of TENG materials. Due to the excellent DC performance of MP-TENG, 1000 LEDs and 54 bulbs can be easily lighted up without any flickers, and commercial electronics can be driven continuously to work stably. This work provides a paradigm shift to achieve high-output constant direct-current, which has widespread application prospects in the field of energy harvesting.

Broader context

With the rapid development of the Internet of Things, a large amount of information is provided through widely distributed sensors and microelectronic devices, which has greatly facilitated and enriched our lives. However, environmental pollution caused by the widespread use of batteries for supporting this huge information network has become increasingly severe. A possible solution is to make each device self-powered by harvesting energy from environment through using triboelectric nanogenerator. However, the further practical applications of TENGs are restricted by their pulsed outputs with high crest factor. In this work, a multi-phase TENG (MP-TENG) with a constant DC outputs and high average output power is prepared only through simple electrode division and circuit connection method. Moreover, electrode misalignment (EM) is first proposed to further improve the output of MP-TENG. Such TENG with ultra-low crest factor can easily light up 1000 LEDs and 54 bulbs without any flickers, and can also drive continuously commercial electronics to work stably. Our systematic research presents that this MP-TENG with merits of both low crest factor and wide selection range of materials, as well as stable DC outputs may significantly promote the practical applications of TENGs in energy harvesting.

Introduction

Triboelectric nanogenerator (TENG), as a promising and effective technology that converts ambient mechanical energy into electricity, provides a new approach for the realization of internet of things (IoTs)[1-3]. Based on the coupling of triboelectrification and electrostatic induction[4, 5], the TENGs exhibit superiorities of cost-effectiveness, easy fabrication, high efficiency, lightweight, and wide choice of materials[6-8]. Among four basic working modes of TENG[9], the freestanding mode usually achieves the highest energy conversion efficiency and represents the easiest way to scavenge regular motion energy through advanced structural design[10-13]. Moreover, the output power of freestanding TENG can be enhanced by fining the grids of constructed grating structure[14]. But the grid size of the freestanding layer with the material of metal or

a. CAS Center for Excellence in Nanoscience, Beijing Key Laboratory of Micro-nano Energy and Sensor, Beijing Institute of Nanoenergy and Nanosystems, Chinese Academy of Sciences, Beijing 100083, P. R. China. E-mail: jiangtao@binn.cas.cn
b. School of Nanoscience and Technology, University of Chinese Academy of Sciences, Beijing 100049, P. R. China.
c. CUSPEA Institute of Technology Wenzhou, Zhejiang 325024, P. R. China
d. School of Materials Science and Engineering, Georgia Institute of Technology, Atlanta, GA 30332-0245, USA. E-mail: zhong.wang@mse.gatech.edu
† Electronic Supplementary Information (ESI) available.
See DOI: 10.1039/x0xx00000x
‡ These authors contributed equally to this work.

polymer is often matched with the electrode size[15], and increasing the grid number a lot will lead to very small central angle[16]. In such case, the fabrication of segmented freestanding layer using synthetic polymers or natural materials is rather challenging, severely limiting the choice of available materials. And using the metal materials with less outstanding electropositivity also restricts the improvement in output power[17].

A significant limitation of TENGs for practical applications is that the generated instantaneous pulse signals have a large ratio of peak value to root-mean square (RMS)/effective value (defined as the crest factor, $CF = I_{max} / I_{RMS}$), which may be even larger than 6[18, 19]. It is a key metric of the power supply's ability to drive a load without distortion. For example, the crest factors of constant direct current (DC) and commercial alternating current (AC) are 1.00 and 1.41, respectively. Such TENGs with a high crest factor cannot power small electronics directly and are unfavorable for charging batteries/supercapacitors, because of exceptional energy losses and decreased energy storage efficiency[20]. Therefore, stable DC generating systems are desirable to be developed to overcome the limitations for practical applications, and make charging of batteries as we do in general cases without a power management system.

In previous works, intensive exploration has been dedicated to generating DC, especially constant DC, through the methods of phase coupling[18, 20-22], electrostatic breakdown[23] and sliding Schottky nanocontact[24]. For ensuring the stable outputs of TENG based on electrostatic breakdown, it is crucial to form and maintain the tiny gap between the charge collection electrode and tribo-material, which has high requirements for the manufacturing process[23, 25]. In addition, for the continuous DC output realized by the sliding Schottky nanocontact technique, the output voltage is too low (~ 8 mV) to power electronics directly[24, 26]. Therefore, many attempts have been devoted to achieving constant DC with decreased crest factor through the phase coupling. An approach of integrating multiple TENGs in parallel, each of which was connected to an individual rectifier, was utilized to greatly decrease the crest factor of current to 1.31[20], while that of paralleled TENGs connected with only one rectifier is larger than 6. Moreover, for a rotating TENG, asymmetrical spatial arrangement between rotator and stator was explored to generate regular phase-shifted alternative currents[18, 22]. After the full-wave rectification and superimposition, the crest factor of current was decreased to 1.26 and 1.1. However, the complex structure design and higher speed requirements make it difficult to envisage for practical scenarios. Besides, the crest factor can be further decreased to 1.08 by a phase coupling approach through introducing multiple phases and groups in a cylindrical TENG[21]. But a problem exists, that is, the average output power drops sharply with increasing the phase number. These previous reports indicate that it is urgent to develop a universal TENG design with low crest factor on the premise of maintaining high output performance.

Herein, a rationally segmented multi-phase triboelectric nanogenerator (MP-TENG) with high performance and low crest factor was developed through an extremely simple manufacturing method. Each electrode of traditional TENG was divided into several pieces, and multiple phases were formed by independently connecting each electrode pair. After rectifying the TENG units with phase difference separately and superimposing them in parallel, the MP-TENG can convert mechanical energy into high DC electrical outputs. The influence of the phase number on the output current

and transferred charges at a low torque of 0.05 N·m was systematically discussed. The crest factor of the current can be greatly reduced to 1.05 for the TENG with above 6 phases, while the 2-phase TENG with a relatively higher crest factor can achieve maximum average output power, which is increased by 40.1% relative to common TENG. Moreover, the crest factor and output power of the 2-phase TENG can be further improved by a novel electrode misalignment method. Due to the stable DC outputs of the MP-TENG, 1000 LEDs and 54 bulbs were lighted up without any flickers. Electronic devices such as watches and calculators were also powered continuously and directly without storage capacitors. Finally, a self-powered motion monitoring system was established by harvesting rotational mechanical energy, demonstrating the widespread applications of the MP-TENG for power sources.

Results and discussion

Structure and working principle of MP-TENG. The structure and working principle of a universal MP-TENG are schematically shown in Figure 1. Taking the rotating MP-TENG with 4 phases (4P-TENG) as an example, the exploded view in Figure 1a presents the hierarchical structures of the rotator and stator. The rotator consists of four sectored rabbit furs arrayed in a circle on the acrylic substrate. And the stator fabricated by printed circuit board (PCB) technology is made up of 32 sector-shaped copper electrodes, which are attached by polytetrafluoroethylene (PTFE) film. Different from a common freestanding TENG structure completely, the grid number of the rotator is no longer half of the number of complementary electrodes in the stator. One power generation unit of the MP-TENG is composed of one fur grid in the rotator and 4 pairs of highlighted multi-color electrodes of the stator (respectively blue, orange, green and red) to distinguish from other units (The electrode color of the other units is gold), as shown in Figure 1a. The highlighted electrodes sharing the same color are defined as one phase of the 4P-TENG. Different from Ryu et al.[18], where the continuous movement of the triboelectric materials with different triboelectric properties causes the electric potential change of at each electrode to generate one signal, thereby forming multiple phases through many electrodes, the basic working mechanism of the MP-TENG obtained through rational electrode division is illustrated in Figure 1b. The triboelectrification between the fur brushes and PTFE film generates positive electrostatic charges on the furs and negative charges on the PTFE surface with equivalent charge amounts. In the initial state (state i), sectored furs, that can be replaced by any other triboelectric material, cover the 4 electrodes completely. When the rotator moves a distance corresponding to one electrode width, due to the electrostatic induction, electrons flow between the first pair of electrodes (blue) through an external circuit. Similarly, with the movement of the rotator, the second-fourth pairs of electrodes (orange, green, red) will generate sequentially charge flow and then uninterruptedly output electrical energy (states ii-iv).

In such TENG structure, the grid size of the rotor does not have to be the same as the electrodes, greatly expanding the material's selection range of TENGs (Figure 1c). All the triboelectric materials can be sourced from the nature according to specific needs to facilitate degradation[27], including cellulose, rice paper, and silk

Journal Name

ARTICLE

fibroin, etc. The cellulose can be extracted from natural plants, such as wood and cotton, while the rice paper and silk fibroin can be collected from wheat and cocoon, respectively. Furthermore, any common material with good triboelectric property can be applied as you want, such as animal furs, fabrics[25] and synthetic polymers[28, 29], without considering the issue of miniaturization. Besides, the working process of the MP-TENG was also confirmed through the

finite element simulations by COMSOL, reflected by the change of the potential difference between the two electrodes, as shown in Figure 1d and Fig. S1 (ESI†). The results show such structure can achieve electrical outputs with a regular phase difference, which is essential for generating DC outputs with low crest factor.
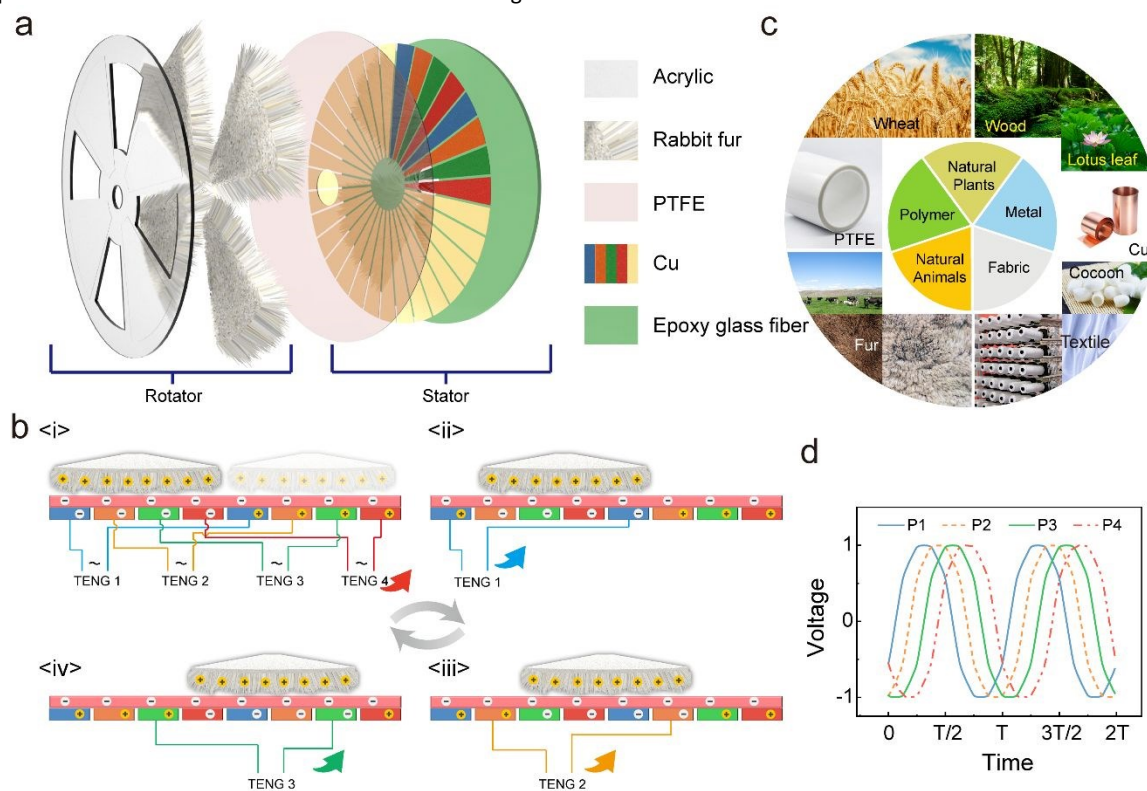

Fig. 1 Architecture and mechanism of the MP-TENG. (a) Schematic diagram of hierarchical structure in the rotating MP-TENG with 4 groups and 4 phases. (b) General working principle of the 4P-TENG. (c) Materials of rotator originating from the nature with wide raw material sources. (d) Normalized triboelectric potential difference of each phase as a function of the rotating period of the rotator obtained by the simulations.

Electrical characterizations for the MP-TENG. A sliding MP-TENG made of copper film with regular shape was designed to reveal the output characteristics of such TENG structure. The schematic diagrams of the power generation units for the 1P- and 4P-TENG are shown in Figure 2a-b, using the copper film and PTFE as the triboelectric materials. The main difference of the two TENGs is the number and width of the electrodes in the stationary part. A sponge was added between the copper film and acrylic substrate to optimize the contact intimacy between tribo-layers. The detailed fabrication processes of the devices are presented in the Experimental Section. In the experiments, the slider was driven by a linear motor to achieve linear reciprocating motions at a frequency of 3 Hz and a pressure of 15 N. Noted that when adjusting the phase number from 1P to 9P, the electrodes of the stationary part have fixed total effective area, and the slider is identical. The moving distance of the slider was set to be 18 mm to form a complete cycle, which is the width of the slider electrode.

The output current and transferred charge of the single-phase TENG and MP-TENG with 4 groups of power generation units

(defined as 4GMP-TENG) were measured and compared, as shown in Figure 2c-f and Fig. S2 (ESI†). Generally, the short-circuit current (I_{SC}) and transferred charge (Q_{SC}) for a freestanding-mode TENG can be expressed as[30]:

$$I_{SC} = dQ_{SC}/dt \qquad (1)$$

$$Q_{SC} = \sigma S/(1 + C_r) \qquad (2)$$

where σ is the surface charge density, S is the contact area, and C_r is the ratio of formed capacitances between different electrodes and the same slider. It can be seen that the current values are determined by the charge density, contact area and time. So, the output current of each phase of 4G4P-TENG is close to that of the 4G1P-TENG, which can reach about 6.59 µA. But the total transferred charge amount of 692 nC for the 4G4P-TENG is larger than the 466 nC of the 4G1P-TENG by calculating the accumulated value of the short-circuit transferred charges of each phase. Moreover, with increasing the phase number, the 4G9P-TENG exhibits the highest outputs of 1016 nC (Figure 2g). This is because, due to the edge effect, the slider with the same size induces a

ARTICLE

<div style="text-align: right">**Journal Name**</div>

relatively higher transferable charge density between smaller electrode pairs compared to electrode pairs of single-phase TENG[31]. When rectifying each phase separately and integrating them in parallel, the superposed current with 9 phases rises to 9.6 μA, which is an enhancement of 46.0% relative to the 4G1P-TENG (Figure 2h and Fig. S3) (ESI†). In addition, the charge accumulation rate of the 9P-TENG is increased by 74.9% (Figure 2i), demonstrating excellent application potential compared with traditional single-phase TENG. Note that the output of each phase

of the MP-TENG is not exactly the same, especially for the 9P-TENG with a smaller electrode width, resulting from the edge effect of edge electrodes (Fig. S4) (ESI†). Also the acceleration and deceleration time of the slider driven by the linear motor becomes non-negligible during the reciprocating motion for smaller electrodes. And choosing a rotating MP-TENG structure can effectively avoid this problem.
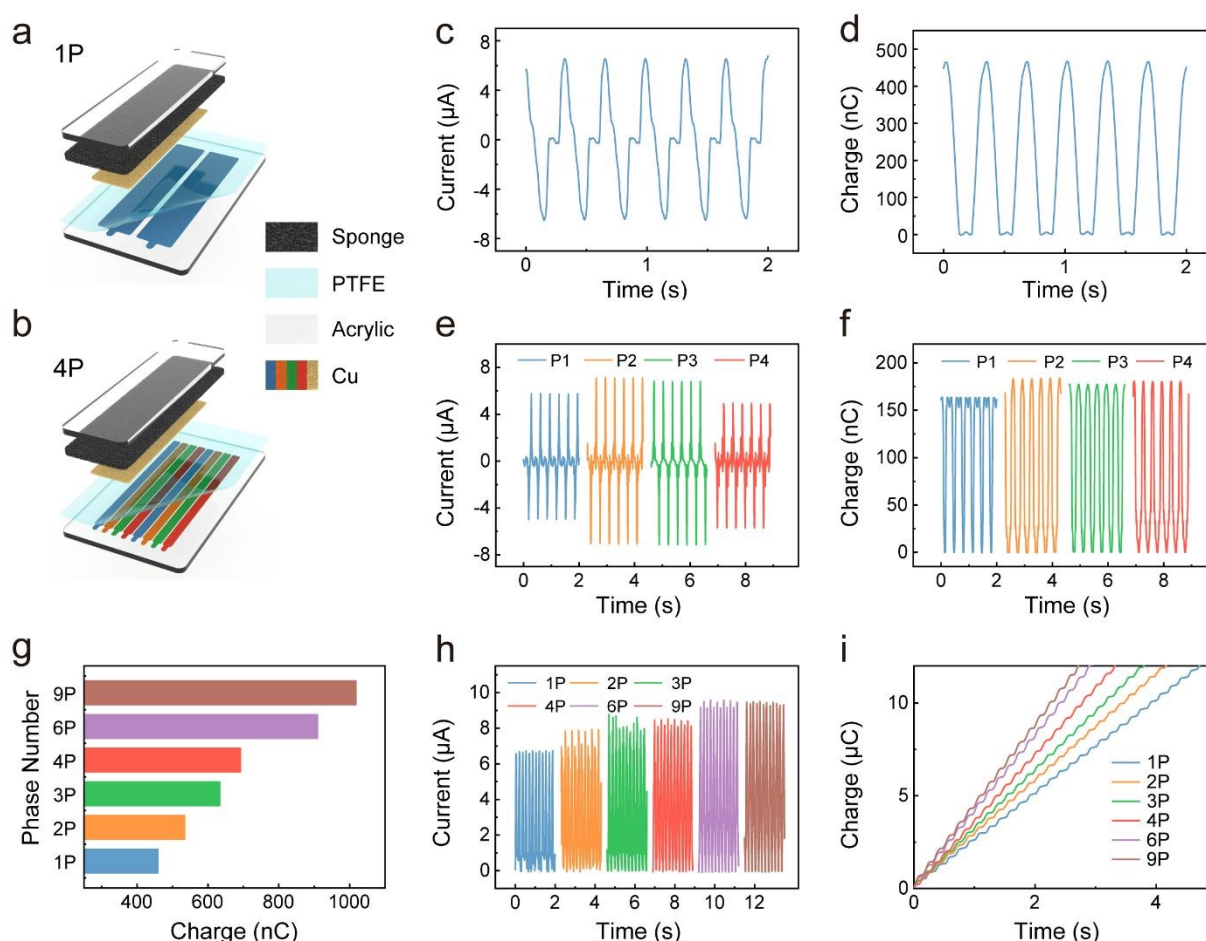

Fig. 2 Influence of phase number on the output performance of sliding MP-TENG at the frequency of 3 Hz. Schematic diagram of the structural unit of (a) 1P-TENG and (b) 4P-TENG. (c) Output current and (d) transferred charge of the 4G1P-TENG. (e) Output current and (f) transferred charge for each phase of the 4G4P-TENG. (g) Transferred charge of 4G-TENG with various phase numbers. (h) Rectified current of the 4G-TENG with respect to the phase number. (i) Accumulated charge amount of the TENG with different phase numbers.

A rotary disk multi-phase TENG, which can eliminate the edge effect of edge electrodes in the sliding type, was designed. The output performance of the rotating MP-TENG with copper as rotor material for different phase numbers was measured on a standardized dynamic torque measurement system, and the results at a torque of 0.2 N·m are shown in Fig. S5 (ESI†). Similar to our previous work, the rotating speed and torque were controlled by the motor and XY-direction platform that can be accurately positioned[32]. The output of each phase is relatively uniform compared to the sliding MP-TENG. Then, like Chen et al.[32], rabbit

furs with excellent electropositivity were used as the rotor material for lowering the material wear and improving durability. The torque was chosen as 0.05 N·m in the following experiments, a value that can be easily overcome by ambient mechanical energy sources, such as wind, water flow, etc. Figure 3a shows the instantaneous transferred charges of each phase for the 4G4P-TENG (Figure 1a) with rabbit furs as the rotor material, which was measured synchronously at 300 rpm. A phase difference of π/n can be observed between adjacent phases (n is the phase number), which is in agreement with the previous simulations, and the transferred

charges and output current of each phase remain consistent. The results are similar for the MP-TENG with other phase numbers (Fig. S6, ESI†). Thus, an almost DC output can be obtained by connecting each phase with full-wave rectifier bridges and superposing them in parallel, as presented in Figure 3b.

Subsequently, the influence of the phase number on the DC outputs was investigated. As the phase number increases from 1 to 9, more stable DC outputs can be achieved, and the crest factor reduces from 1.3 to 1.05 (Figure 3c-d and Fig. S7, ESI†). The amount of charge accumulation per second is also increased from 13.8 to 21.26 μC, and the RMS value of the DC current arrives at 21.28 μA, which are increased by 54.1% and 42.1%, respectively (Figure 3e). Figure 3f shows the average power behaviors with respect to the load resistance for the rotating MP-TENG with different phases. The average power can be calculated by

$$P_{ave} = \frac{\int_0^T I(t)^2 R dt}{T} \tag{3}$$

where the $I(t)$ is the current across the resistor at the time t, R is the resistance, and T is the period. It can be found that a maximum average power of 8.98 mW can be obtained for the 4G1P-TENG, while the 4G2P-TENG can reach 12.58 mW, achieving an increase of 40.1%. The corresponding average power density is 1.11 W·m^{-2} at the adopted torque condition. It is the result of the combined effect of the edge effect for smaller electrodes and the reduction of the generator capacitance due to its structure[31]. The matched resistance increases slightly from 60 MΩ to 90 MΩ with the increasing of phase number, which is also consistent with the previous studies[14]. Here, a new record of ultra-low crest factor of 1.05 for DC-TENG with multiphase coupling is achieved, whose maximum average power of 271 mW·m^{-2}·Hz^{-1} is quite competitive at the torque of only 0.05 N·m (Figure 3g, Fig. S8 and Table 1, ESI†). Besides, the average power and output current can also be improved by increasing the number of groups, the rotating speed and torque[32], as shown in Figure 3h and Fig. S9-10 (ESI†).

Based on the excellent DC output performance of our MP-TENG, 1000 LEDs and 54 commercial bulbs can be lighted up easily without any flickering, which indicates that the outputs have extremely low current ripple, as demonstrated in Figure 3i-j and Supplementary Movie 1-2. The high-quality DC output signals produced by the MP-TENG make it safe for the electronic equipment. Moreover, when powering lighting equipment, the stroboscopic effect that is unpractical for human use and damages to human eyes can be avoided. In addition, the high output DC of the MP-TENG enables it to directly drive small electronics without any energy storage component. An electronic watch and a commercial calculator can work continuously by using the 4G4P-TENG at the rotating speed of 30 rpm and 150 rpm respectively, at a low torque of 0.05 N·m (Figure 3k-l and Supplementary Movie 3-4). These demonstrations illustrate the broad practical application prospects of MP-TENG in our daily lives.
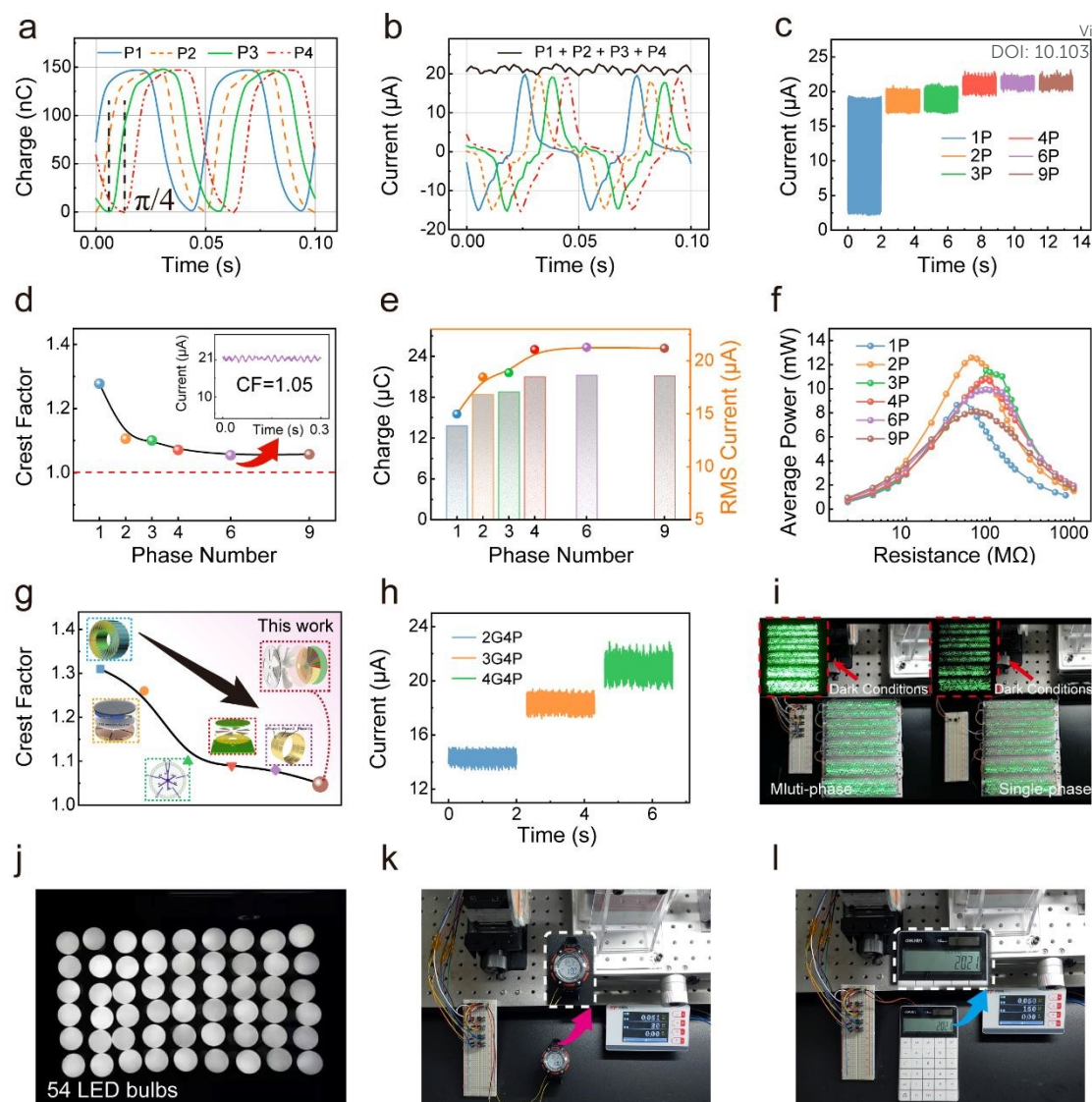
Fig. 3 Output performance of the rotating MP-TENG with rabbit furs as the rotor material at a torque of 0.05 N·m. (a) Transferred charge of each phase for the 4G4P-TENG under simultaneous measurements. (b) Output current of each phase and the rectified and superposed output of 4G4P-TENG. (c) Output current after rectification and superposition of each phase output for the 4G-TENG with different phase numbers at the rotating speed of 300 rpm. (d) Crest factor of the rectified and superposed current for the MP-TENG with different phase numbers. The inset shows the output current of 4G6P-TENG. (e) Accumulated charge amount per second and the RMS value of rectified current with respect to the phase number. (f) Average power-resistance relationships for the MP-TENG with different phase numbers. (g) The crest factor of this work compared with that reported by others. (h) Comparison of the rectified superposed current of the 4P-TENG with different groups at 300 rpm. (i-j) Comparison of DC output characteristics of multi-phase and single-phase TENGs, where (i) 1000 LEDs and (j) 54 LED bulbs can be lighted up easily by the 4G4P-TENG without any flickers. (k) Photograph of an electronic meter driven directly by the 4G4P-TENG at 30 rpm. (l) Photograph of a commercial calculator powered by the MP-TENG at 150 rpm to work stably.

Electrical characterizations for the EMMP-TENG. According to the above study, the two-phase TENG produces the highest output power, but the crest factor of its output current remains at a relatively high level. Here, a method of electrode misalignment (EM) was proposed for the first time to solve this issue, as schematically shown in Figure 4a. For the normal two-phase TENG contains two groups of power generation units (2G2P, Figure 4a-i), the EM degree was represented by the displacement of the right slider moving forward toward the left slider, which was chosen as 1/3, 1/2, 3/4 of one electrode width (Figure 4a-ii-iv). At such situations, the four TENGs become different, and the phase number is changed from 2 to 4. The signals generated by two units without electrode misalignment are completely synchronized, namely No. 1 and No. 3, No. 2 and No. 4, as indicated in Figure 4b and Fig. S11a-b (ESI†). However, with the EM, the forward movement of the right slider changes the phases of No. 3 and No. 4 signals. Therefore, there exists a phase difference between the 4 sets of current signals according to the EM degree (Figure 4c), which can also be verified

by the simulated voltage profiles of the four phases (Fig. S11c, ESI†). The detailed working mechanism for the electrode misaligned MP-TENG (EMMP-TENG) can be seen in Fig. S12 (ESI†), and the measured output voltage, current and transferred charge of each phase was compared for the normal MP-TENG and EMMP-TENG with 1/3 electrode misalignment (Fig. S13, ESI†). Owing to the phase difference, the crest factor of the rectified superposed current drops markedly from 1.15 to 1.05, when the slider moves forward by 1/3 of one electrode width (Figure 4d-e). The enlarged diagram of the output current in Figure 4e also proves this point.

The average power of EMMP-TENG with different EM degrees as a function of the load resistance was plotted, indicating an increase of 19.5% for 2G4P-TENG with 1/3 electrode misalignment relative to the normal 2G4P-TENG without EM (Figure 4f). Also, the

charging speed to a fixed capacitor was found to be increased by 9.7% (Fig. S14, ESI†). As we can see, a more stable DC output with lower crest factor can be realized only through simple slider/rotor position change and circuit connection on the premise of high output power, which is essential to the practical applications of MP-TENG. Here, common materials in our daily life have been selected and used, such as wood, nylon fabrics, printer paper, and polyester fabrics, for comparison with the results of using the rabbit furs. Interestingly, all MP-TENGs with these materials show excellent DC output performance (Figure 4g), and the crest factor for all materials can be reduced to be below 1.1 when the electrode is misaligned (Figure 4h). The rabbit fur material can achieve the lowest crest factor of 1.05. These results demonstrate the wide applicability of our EMMP-TENG structure.
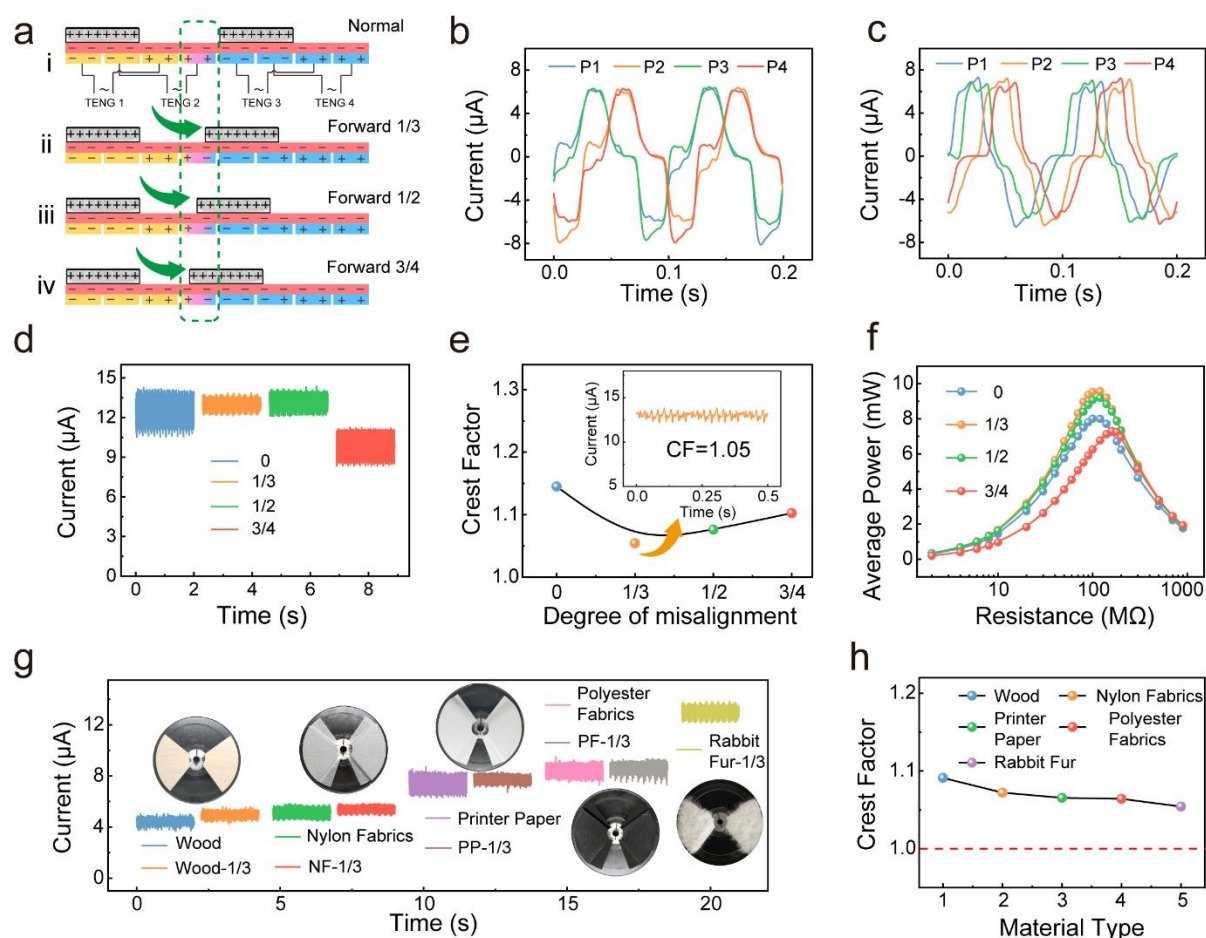

Fig. 4 Mechanism and output performance of electrode misaligned MP-TENG. (a) Schematic diagram of electrode misaligned MP-TENG designed with different degrees of misalignment. (b-c) Output current of each phase for the 2G4P-TENG (b) without electrode misalignment and (c) with 1/3 electrode misalignment under simultaneous measurements. (d-e) Influence of different electrode misalignment degrees on the (d) rectified superposed current and (e) crest factor. An enlarged view of the output current for the TENG with 1/3 electrode misalignment is shown in the inset of figure e. (f) Average output power with respect to the load resistance for the MP-TENG with different electrode misalignment degrees. (g) Output current of the EMMP-TENG made of a variety of common materials after electrodes are dislocated (wood, nylon fabrics, printer paper, polyester fabrics, rabbit fur, etc.). (h) Crest factor of the output current for the EMMP-TENG with different materials.

Application of EMMP-TENG. With the increasing attention to environmental pollution, the realization of a lifestyle relying on smart electronics, powered by clean and renewable energies, has become an objective for lots of consumers. However, in the smart world of IoTs, the power supply problem arising from widespread sensors has always been an insurmountable gap in the process of realizing a both smarter and greener life. Although solar cells and electromagnetic induction-based equipment can meet some requirements, these technologies will undoubtedly be affected by the weather or have the fatal problems of high frequency requirements and bulky equipment. Besides, the TENG technology that can collect mechanical energy from its own motion is also limited by the high crest factor of outputs. The EMMP-TENG we designed based on the principle of electrode misalignment and fur brush, exhibiting the advantages of lower crest factor, higher charging efficiency and more stable output, is expected to solve this problem. It is worth noting that the EMMP structure can be applied to any rotation or even sliding motion (Figure 2), including the wind and water drop driven motions, due to its easy manufacturability. Figure 5a is a schematic diagram of proposed concept for smart green travel based on the EMMP-TENG.

Here, to demonstrate the application of the EMMP-TENG in environmental energy harvesting, a 2*2G4P EMMP-TENG through connecting two sets of 2G4P units in parallel was fabricated and installed on an ordinary bicycle to collect the energy of braking or spinning (Figure 5b). The detailed structural settings can be found in Fig. S15 (ESI†). During the riding, the RMS value of the rectified superposed current for the EMMP-TENG can reach 27.85 μA, and the crest factor can be stabilized at about 1.05 (Fig. S16, ESI†). The charging performance of the device to various capacitors was also explored, as presented in Figure 5c. The voltage on the capacitor of 470 μF can be charged to 3.0 V within 52 s, showing an excellent energy harvesting ability. Due to the excellent performance of the EMMP-TENG, a self-powered wired cyclocomputer can work continuously by collecting energy from the rotation of the wheels. It can display instantaneous speed and other parameters, such as total riding distance and calorie consumption, etc. Interestingly, the voltage on the capacitor keeps increasing as long as you keep riding (Figure 5d and Supplementary Movie 5), which means that the energy harvesting speed exceeds the consumption speed. We believe that the performance will become more outstanding by introducing the power management[33]. Moreover, a wireless cyclocomputer consisting of a signal transmitter and a receiver can also be driven through charging the capacitor (Figure 5e, Fig. S17, and Supplementary Movie 6-7, ESI†). This device can be easily assembled and provide a stable power supply in other application scenarios. For example, it can be installed on street lamps or flagpoles to collect wind energy[34], or installed in water channels to collect water flow energy. These will further promote the realization of a sustainable smart life.
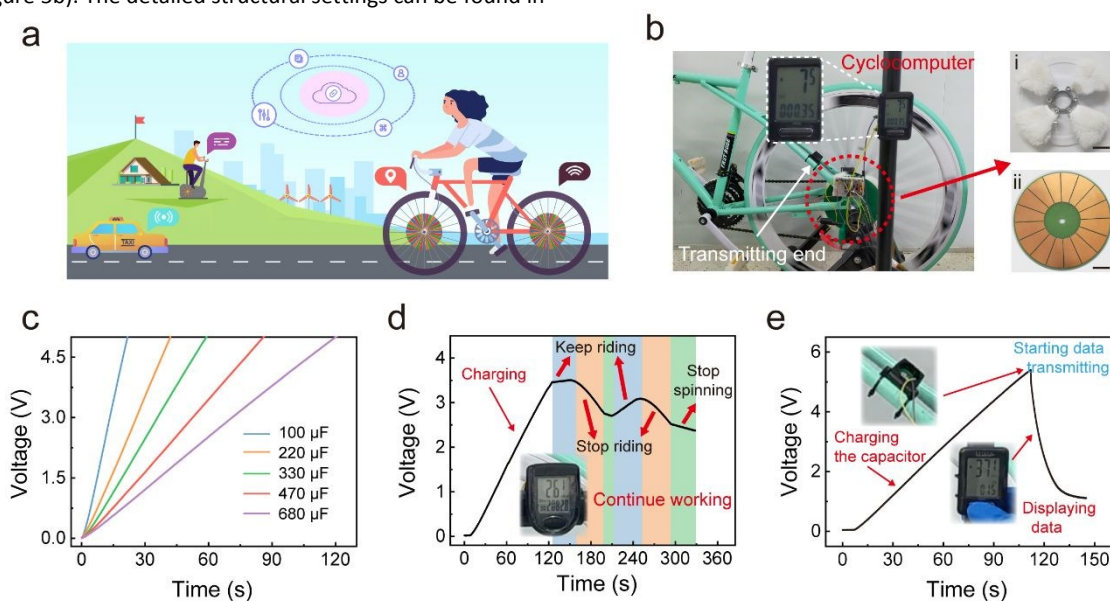

Fig. 5 Application of the EMMP-TENG for collecting rotational mechanical energy. (a) Proposed concept of applying the EMMP-TENG in smart green travel. (b) Digital photo of ordinary bicycle equipped with the EMMP-TENG (two sets of 2G4P units) on its rotating part and a cyclocomputer for facilitating the demonstration. The photographs of the (i) rotor part and (ii) stator part are also shown (scale bar: 3 cm). (c) Charging curves of the EMMP-TENG to various capacitors at manual speed. (d) Charging and discharging processes for a 680 μF capacitor to power the wired cyclocomputer, which can continue working stably as long as one keeps riding. The inset shows the photograph of the wired cyclocomputer at the working state. (e) Voltage profile on a 470 μF capacitor charged by the EMMP-TENG to power the signal transmitter, which can measure the rotating speed and transmit it wirelessly to the cyclocomputer in real time.

Conclusions

In summary, we have constructed a MP-TENG only through simple electrode division and circuit connection method, which exhibits merits of both low crest factor and wide selection range of materials, as well as stable DC outputs. The rotor grids do not have to match with the electrodes in size, greatly simplifying the manufacturing process of TENG and expanding the selection scope of materials. The materials that are common in our daily life, such as wood and cloth fabrics, can be easily used to generate DC-like

output with a crest factor of less than 1.1. Moreover, an almost constant DC output with ultra-low crest factor of 1.05 and an average power increase of 40.1% can be achieved through rectifying and superimposing TENGs with phase difference in parallel. These characteristics make the design of the EMMP/MP-TENG a universally applicable design. Based on the stable DC electrical outputs of the MP-TENG, 1000 LEDs and 54 bulbs can be lighted up easily without any flickers at the torque of only 0.05 N·m. And the commercial electronics, such as wearable electronics and cyclocomputers, can also be driven continuously to work. This work provides a new and valid strategy for high output direct-current, showing a wide range of application prospects.

Experimental

Fabrication of Sliding MP-TENG

Two pieces of acrylic boards with a dimension of 16.4 cm × 9.5 cm × 5 mm were cut by using a laser cutter (PLS6.75) as substrates. For each structural unit of the slider, a copper film of 18 mm × 75 mm × 35 μm with a chamfer of 1 mm, was adhered to a 5 mm-thick sponge that was glued onto an acrylic substrate for improving the material contact. For the stator, the epoxy glass fiber substrate with copper layers (35 μm in thickness) was fabricated by the PCB technique. Each group of electrodes was divided into several pieces to form multiple phases. For example, the electrode number of 4P-TENG is 8 in each group, and each electrode has a chamfer of 1 mm, a length of 75 mm, and a width of 3.85mm. Note that, when varying the phase number, the total electrode area was guaranteed to be the same. Then an 80 μm-thick PTFE film was adhered on the copper layers as the triboelectric layer.

Fabrication of Rotating MP-TENG

The rotating MP-TENG is composed of two parts: a rotor disk with different materials and a stator electrode disk. For the disk with rabbit furs, as an example, four sectored furs with equal-degree radially-arrayed sectors (4G) were pasted on the acrylic substrate. The outer diameter and inner diameter of the sectored furs are 120 mm and 23 mm, respectively, similar to the previous work. The same acrylic substrate and 9 mm-long rabbit furs were used in this work. Similarly, other materials, such as wood and nylon fabrics, were cut into the target shape by laser cutter and then glued to the acrylic substrate together with the sponge. For the electrode disk with different electrode numbers fabricated by PCB technology, the inner and outer diameters are the same as the rotor disk. All electrode materials are the same, copper. Moreover, regardless of the phase number, the entire electrode area was fixed as well as the sliding MP-TENG. Finally, an 80μm-thick PTFE film was adhered on the copper layers as the triboelectric layer.

Fabrication of Rotating EMMP-TENG

The fabricated method of EMMP-TENG is similar with the rotating

MP-TENG. The only difference is that the positions of rotor sectors with different materials are changed to form an electrode misalignment.

Electric Measurements of the TENG Device

The sliding motion was conducted by a linear motor (TSMV120-1S), and the rotary motion was carried out by a rotational motor (60ST-M01930). The torque was measured by a commercial torque sensor (DYN-200). The torque used in the experiments is 0.2 N·m for all materials except for the rabbit fur brush which adopts 0.05 N·m. The transferred charge and output current were measured by several current preamplifiers (Keithley 6517 System Electrometer), while the output voltage was measured using a high-voltage probe (internal impedance: 500 MΩ) and a mixed domain oscilloscope (HVP, Tektronix MDO3000s).

Author contributions

P.C. and Z.L.W. conceived the idea. T.J. and Z.L.W. conducted the work and supervised the experiments. P.C. and T.J. prepared the manuscript. P.C. designed and fabricated the device and performed the electrical measurements. J.A. and R.C. helped for the electrical measurements and application demonstration. S.S. assisted with the experiments. A.B. helped modify the manuscript. All the authors discussed the results and commented on the manuscript.

Conflicts of interest

The authors declare no competing financial interest.

Acknowledgements

References

1. R. Hinchet, H.-J. Yoon, H. Ryu, M.-K. Kim, E.-K. Choi, D.-S. Kim and S.-W. Kim, *Science*, 2019, **365**, 491.

2. C. Rodrigues, D. Nunes, D. Clemente, N. Mathias, J. M. Correia, P. Rosa-Santos, F. Taveira-Pinto, T. Morais, A. M. Pereira and J. Ventura, *Energy Environ. Sci.*, 2020, **13**, 2657-2683.

3. W. Xu, H. Zheng, Y. Liu, X. Zhou, C. Zhang, Y. Song, X. Deng, M. Leung, Z. Yang, R. X. Xu, Z. L. Wang, X. C. Zeng and Z. Wang, *Nature*, 2020, **578**, 392-396.

4. Z. L. Wang, *Mater. Today*, 2017, **20**, 74-82.

5. F.-R. Fan, Z.-Q. Tian and Z. Lin Wang, *Nano Energy*, 2012, **1**, 328-334.

6. Y. Zi, H. Guo, Z. Wen, M. H. Yeh, C. Hu and Z. L. Wang, *ACS Nano*, 2016, **10**, 4797-4805.

7. J. Xiong, P. Cui, X. Chen, J. Wang, K. Parida, M. F. Lin and P. S. Lee, *Nat Commun*, 2018, **9**, 4280.

8. H. Guo, J. Chen, L. Wang, A. C. Wang, Y. Li, C. An, J.-H. He, C. Hu, V. K. S. Hsiao and Z. L. Wang, *Nature Sustainability*, 2020, **4**, 147-153.

9. Z. L. Wang, J. Chen and L. Lin, *Energy Environ. Sci.*, 2015, **8**, 2250-2282.

10. Y. Xie, S. Wang, S. Niu, L. Lin, Q. Jing, J. Yang, Z. Wu and Z. L. Wang, *Adv Mater*, 2014, **26**, 6599-6607.

11. H. Fu, X. Mei, D. Yurchenko, S. Zhou, S. Theodossiades, K. Nakano and E. M. Yeatman, *Joule*, 2021, **6**, 1-45.

12. W. He, W. Liu, J. Chen, Z. Wang, Y. Liu, X. Pu, H. Yang, Q. Tang, H. Yang, H. Guo and C. Hu, *Nat Commun*, 2020, **11**, 4277.

13. R. Lei, Y. Shi, Y. Ding, J. Nie, S. Li, F. Wang, H. Zhai, X. Chen and Z. L. Wang, *Energy Environ. Sci.*, 2020, **13**, 2178-2190.

14. G. Zhu, J. Chen, T. Zhang, Q. Jing and Z. L. Wang, *Nat Commun*, 2014, **5**, 3426.

15. J. Cheng, W. Ding, Y. Zi, Y. Lu, L. Ji, F. Liu, C. Wu and Z. L. Wang, *Nat Commun*, 2018, **9**, 3733.

16. T. Jiang, X. Chen, C. B. Han, W. Tang and Z. L. Wang, *Adv. Funct. Mater.*, 2015, **25**, 2928-2938.

17. H. Zou, Y. Zhang, L. Guo, P. Wang, X. He, G. Dai, H. Zheng, C. Chen, A. C. Wang, C. Xu and Z. L. Wang, *Nat Commun*, 2019, **10**, 1427.

18. H. Ryu, J. H. Lee, U. Khan, S. S. Kwak, R. Hinchet and S.-W. Kim, *Energy Environ. Sci.*, 2018, **11**, 2057-2063.

19. X. Liang, T. Jiang, G. Liu, Y. Feng, C. Zhang and Z. L. Wang, *Energy Environ. Sci.*, 2020, **13**, 277-285.

20. X. Li, X. Yin, Z. Zhao, L. Zhou, D. Liu, C. Zhang, C. Zhang, W. Zhang, S. Li, J. Wang and Z. L. Wang, *Adv. Energy Mater.*, 2020, **10**, 1903024.

21. J. Wang, Y. Li, Z. Xie, Y. Xu, J. Zhou, T. Cheng, H. Zhao and Z. L. Wang, *Adv. Energy Mater.*, 2020, **10**, 1904227.

22. R. D. I. G. Dharmasena, H. M. Cronin, R. A. Dorey and S. R. P. Silva, *Nano Energy*, 2020, **75**, 104887.

23. L. Di, Y. Xing, G. Hengyu, Z. Linglin, L. Xinyuan, Z. Chunlei, W. Jie and W. Zhong Lin, *Sci. Adv.*, 2019, **5**, eaav6437.

24. J. Liu, A. Goswami, K. Jiang, F. Khan, S. Kim, R. McGee, Z. Li, Z. Hu, J. Lee and T. Thundat, *Nat Nanotechnol*, 2018, **13**, 112-116.

25. R. Cheng, K. Dong, P. Chen, C. Ning, X. Peng, Y. Zhang, D. Liu and Z. L. Wang, *Energy Environ. Sci.*, 2021, **14**, 2460-2471.

26. J. Liu, F. Liu, R. Bao, K. Jiang, F. Khan, Z. Li, H. Peng, J. Chen, A. Alodhayb and T. Thundat, *ACS Appl Mater Interfaces*, 2019, **11**, 35404-35409.

27. W. Jiang, H. Li, Z. Liu, Z. Li, J. Tian, B. Shi, Y. Zou, H. Ouyang, C. Zhao, L. Zhao, R. Sun, H. Zheng, Y. Fan, Z. L. Wang and Z. Li, *Adv Mater*, 2018, **30**, 1801895.

28. S. Li, Y. Fan, H. Chen, J. Nie, Y. Liang, X. Tao, J. Zhang, X. Chen, E. Fu and Z. L. Wang, *Energy Environ. Sci.*, 2020, **13**, 896-907.

29. S.-F. Leung, H.-C. Fu, M. Zhang, A. H. Hassan, T. Jiang, K. N. Salama, Z. L. Wang and J.-H. He, *Energy Environ. Sci.*, 2020, **13**, 1300-1308.

30. S. Niu, Y. Liu, X. Chen, S. Wang, Y. S. Zhou, L. Lin, Y. Xie and Z. L. Wang, *Nano Energy*, 2015, **12**, 760-774.

31. Z. Wu, S. Wang, Z. Cao, R. Ding and X. Ye, *Nano Energy*, 2021, **83**, 105787.

32. P. Chen, J. An, S. Shu, R. Cheng, J. Nie, T. Jiang and Z. L. Wang, *Adv. Energy Mater.*, 2021, **11**, 2003066.

33. Z. Wang, W. Liu, W. He, H. Guo, L. Long, Y. Xi, X. Wang, A. Liu and C. Hu, *Joule*, 2021, **5**, 441-455.

34. C. Ye, K. Dong, J. An, J. Yi, X. Peng, C. Ning and Z. L. Wang, *ACS Energy Letters*, 2021, **6**, 1443-1452.